

# Measuring spin-polarized electronic states of quantum materials: $2H$ -NbSe<sub>2</sub>

Chiara Bigi<sup>1,2</sup>, Federico Mazzola,<sup>2</sup> Jun Fujii,<sup>2</sup> Ivana Vobornik,<sup>2</sup> Giancarlo Panaccione<sup>1,2</sup>, and Giorgio Rossi<sup>1,2</sup>

<sup>1</sup>*Department of Physics, University of Milano, 20133 Milano, Italy*

<sup>2</sup>*CNR-IOM TASC Laboratory, 34139 Trieste, Italy*



(Received 25 November 2020; revised 29 May 2021; accepted 2 June 2021; published 25 June 2021)

Probing the energy and spin electron properties of materials by means of photoemission spectroscopy gives insights into the low-energy phenomena of matter driven by spin orbit coupling or exchange interaction. The information that can be derived from complete photoelectron spectroscopy experiments, beyond  $E(\mathbf{k})$ , is contained in the photoemission transition matrix elements that determine peak intensities. We present here a complete photoemission study of the spin-polarized bands of  $2H$ -NbSe<sub>2</sub>, a material that presents a surface spin-texture. Circular dichroism in angular-resolved photoemission spectroscopy (CD-ARPES) data are compared with spin-polarized angular-resolved spectra (SARPES) as measured with linearly polarized radiation in a well-characterized experimental chirality, at selected photon energy values. CD-ARPES is due to a matrix element effect that depends strongly on photon energy and experimental geometry: we show that it cannot be used to infer intrinsic spin properties in  $2H$ -NbSe<sub>2</sub>. On the other hand, SARPES data provide reliable direct information on the spin properties of the electron states. The results on  $2H$ -NbSe<sub>2</sub> are discussed, and general methodological conclusions are drawn on the best experimental approach to the determination of the spin texture of quantum materials.

DOI: [10.1103/PhysRevB.103.245142](https://doi.org/10.1103/PhysRevB.103.245142)

## I. INTRODUCTION

The spin polarization (SP) of bulk and surface electronic states in solids is a manifestation of magnetism, spin-orbit coupling (SOC), or proximity effects at ferroic interfaces [1–5]. The need to measure the so called spin-texture of solid surfaces has prompted the application of spin-resolved angular-resolved photoemission spectroscopy (SARPES) to a growing number of quantum materials, aiming to identify the spin properties of topological surface states, or to fully resolve and characterize Rashba split electron states. The exploitation of the matrix element effect (MEE) is performed in circular dichroism (CD-ARPES) experiments yielding highly variable spectroscopic intensities that are of uncertain interpretation in the case of extended states. Here we present a study of the electron states of  $2H$ -NbSe<sub>2</sub> by performing both SARPES and CD-ARPES, approximating a complete photoemission experiment, and we derive unambiguous experimental information on the spin polarization.

In the approximation of low excitation density that is appropriate for a typical synchrotron radiation experiment (at most one photoelectron excited per 10–100 ps light pulse), the measured photoelectron energy spectrum  $I_{\text{ph}}(\mathbf{k}, \omega)$  relates to the one-electron removal spectral function  $A(\mathbf{k}, \omega)$ :

$$I_{\text{ph}} \propto A(\mathbf{k}, \omega) |\langle \varphi_f | H_{\text{int}} | \varphi_i \rangle|^2. \quad (1)$$

The experiment, therefore, can be directly connected with the energy dispersion— $E_B$  versus  $\mathbf{k}$ —of the ground-state electronic structure, its low-energy excitations, and the effects of electronic correlations of the system [6–8]. ARPES has provided in fact the best experimental proof of the band-structure

model of solids and has prompted many-body theory refinements to the electronic structure calculation methods to best approximate the measured energy dispersions and peak widths in  $e$ - $e$  correlated systems. For instance, SARPES results on the three ferromagnetic three-dimensional (3D) transition metals are still a challenge for theoretical computations [9,10]. However, the measured intensity  $I_{\text{ph}}(\mathbf{k}, \omega)$  is weighted by the photoemission matrix element, expressed in the Golden Rule formalism as  $|\langle \varphi_f | H_{\text{int}} | \varphi_i \rangle|$ . This *effective transfer function* represents the probability of the electron transition from the initial to the final photoelectron state through the interaction operator  $H_{\text{int}}$ , which can be expressed with the dipole operator in the low excitation density frame. Consequently, both the excitation energy  $h\nu$  and the light polarization ( $\hat{e}$ ) enter the matrix element affecting the photoemission intensity. Finally, the complete set of parameters and symmetries of the experiment are reflected in the measured intensities, including the detailed geometry of the experimental setup. The MEE refers to such an effective transfer function of the  $A(\mathbf{k}, \omega)$  into detected photoemission intensity maps. The SP analysis of the energetically and angularly selected photoelectrons can be obtained by performing downstream a scattering experiment that detects an asymmetry in the photocurrent intensity as induced by LS coupling (Mott scattering) or exchange interaction (VLEED detection) in a suitable target. Consequently, SARPES is also affected by the MEE of spin-split initial electron states [11–14]. Atomiclike initial states, such as those probed by core-level photoemission, do display SP in ARPES as a consequence of angular momentum conservation, while in fully angle-integrated PES the SP is zero [15–18]. A general expression for the angular distribution of photoelectrons

ejected from polarized atoms includes the partial photoionization cross section  $\sigma_{nlj}(\omega)$  and the parameters reflecting the projection of angular momenta, according to the density matrix formalism of Blum [19]. CD-ARPES and linear magnetic dichroism in ARPES arise from *alignment* and from *orientation* of atoms, as reflected in experiments on core levels with and without SP analysis [20–24].

SARPES has reached, in the past decade, adequate measurement efficiency both with high-energy resolution (5–50 meV) and high momentum resolution as derived from angular resolution ( $0.1^\circ$ – $0.5^\circ$ ) [25–29]. The combination of state-of-the-art electron analyzers and spin polarimeters with tunable VUV or soft-x ray beams of a selectable polarization state can make SARPES a complete photoelectric effect experiment. This is the best suited surface-sensitive method for the study of the extended electronic states of highly correlated quantum materials [30–33]. In a SARPES setup using polarized synchrotron radiation or laser high harmonics sources, one can measure simultaneously all the quantum numbers of the photoelectron final state in vacuum [6,34]. In CD-ARPES of extended states, one measures changes of  $I_{ph}(\mathbf{k}, \omega)$  as a function of helicity of the photoabsorbed light, at one or several values of photon energy, in the given experimental geometry (incident angles, emission angles, and crystallographic plane orientations with respect to the scattering plane). Such measurements can be done with synchrotron radiation sources, using out-of-plane dipole radiation or dedicated insertion devices, as well as with laser sources equipped with quarter-wave plates. CD-ARPES requires us to acquire two datasets, i.e., a factor 2 more effort with respect to unpolarized ARPES. The SP analysis is instead very inefficient, being based on scattering experiments, and it requires  $10^2$  (VLEED) to  $10^4$  (Mott) more measuring time to reach comparable statistics at the same values of energy/angle resolution. This has motivated some attempts to infer the spin properties of the  $A(\mathbf{k}, \omega)$  from CD-ARPES data alone [35–38]. However, the radial extension and shape of the electron states in solids, due to hybridization, do not allow the MEE analysis in terms of atomic wave functions. Evidence of a large MEE is found in  $4d$  and  $5d$  transition elements, e.g., the modulation of the  $4d(5d)$  cross section  $[\sigma_{4d(5d)}(\omega)]$  between its maximum in the VUV and the Cooper minimum that is reduced to less than a factor 10 in the metals, while for isolated atoms, or surface absorbed atoms, is both predicted and measured to be over a factor 100 [39,40]. Large CD-ARPES effects have been reported, e.g., for the ferromagnetic Ni(111) surface [41] for topological insulators, Rashba split peaks in semiconductors, and even in cases of very small SOC as for the Cu(111) Shockley L-gap surface state [41–46]. In spite of this well-documented phenomenology and theoretical analysis, one finds in the literature CD results on topological states in quantum materials being interpreted as evidence of the spin character of the initial extended states either directly [35,47] or indirectly through probing orbital angular momentum [37].

Here we present photoemission results on the transition-metal dichalcogenide (TMDC)  $2H$ -NbSe<sub>2</sub>, which is known to display well-characterized 2D-like spin-polarized states. Based on the acquisition of a complete experimental dataset, we address the issue of consistency of interpretation of SARPES and CD-ARPES data of the electron states of

quantum materials, with general methodological implications.  $2H$ -NbSe<sub>2</sub> has a rich phase diagram, characterized by different electronic order parameters at low temperatures: charge density waves below 33 K [48–50] and superconductivity below 7.2 K [48,51]. The understanding of the NbSe<sub>2</sub> spin properties—and of their interplay with the low-temperature phases of this material—is of interest also for potential relevance in spintronics [52–54]. Here we show that in a well-characterized ARPES setup, as shown in Fig. 1, by using polarized synchrotron radiation in the VUV-XUV range, the measurement of SP of the  $2H$ -NbSe<sub>2</sub> electron states yields consistent results when the photon energy is changed. At the same time, we show how the spin-integrated CD-ARPES data show large  $I_{ph}(\mathbf{k}, \omega)$  features that do not correlate with the SP of the same band states. CD intensity modulations do not reflect the spin polarization of the electronic states of  $2H$ -NbSe<sub>2</sub>: CD-ARPES is found not to be sensitive to the spin texture of the material, which emerges instead only from the SARPES. The SP results, measured in SARPES, are qualitatively robust, i.e., little affected by MEE, and must be considered as the relevant data to address the spin texture of the quantum materials.

## II. RESULTS AND DISCUSSION

Single crystals of  $2H$  polymorph NbSe<sub>2</sub> [55] were oriented by means of Laue diffraction and subsequently cleaved in ultrahigh vacuum and cooled to liquid nitrogen temperature in the SARPES spectrometer of the NFFA APE-LE beamline of the Elettra storage ring in Trieste [56]. The overall experimental resolution was set to 40 meV– $0.2^\circ$  for ARPES and CD-ARPES and to 80 meV– $0.5^\circ$  for SARPES. In a single NbSe<sub>2</sub> layer, the Nb atom is surrounded by six atoms displaced at the vertex of a trigonal prism. The  $2H$  crystal structure presents A-B-A-B stacking of layers, alternatively rotated by  $180^\circ$  as sketched in the side view in Fig. 2(a). The unit cell consists of two subsequent Se-Nb-Se layers. The top view of a single layer shows Nb and Se occupying the alternate sites of the honeycomb lattice. Figure 2 summarizes the electronic band structure measured with 70 eV linearly horizontal (LH) polarized light. The gray area in the Brillouin zone sketch of Fig. 2(a) marks the  $\Gamma$ - $K$ - $M$  plane, which is the one probed by the photon energy ( $h\nu = 70$  eV) considering the inner potential  $V_0 = 17.6$  eV reported in [57] and lattice parameter  $c = 12.55$  Å [55]. The Fermi surface (FS) contours probed by ARPES are shown in Fig. 2(b). Two intense, concentric, trigonally warped contours are centered at the  $K$  and  $K'$  points and have predominantly Nb  $4d$  orbital character, as well as the hexagonal Fermi contour that encircles the  $\Gamma$  point. The signal from the Se  $p_z$  derived Fermi contour centered at the  $\Gamma$  point is faintly visible in the spectra due to unfavorable contrast with respect to the other much more intense bands. In fact, the atomic cross sections of the two orbitals would show a different contrast due to the presence of the Cooper minimum of the Nb  $4d$  wave function around 80 eV. However, the Cooper minimum of the Nb  $4d$  might be reduced by hybridization [40]. The  $4d$  orbital character is mixed by the strong SOC displayed by NbSe<sub>2</sub>. In particular, the Fermi surface close to the BZ center has mainly  $d_{z^2}$  character, while near the zone corners a mixed  $d_{x^2-y^2}/d_{xy}$  character is predominant

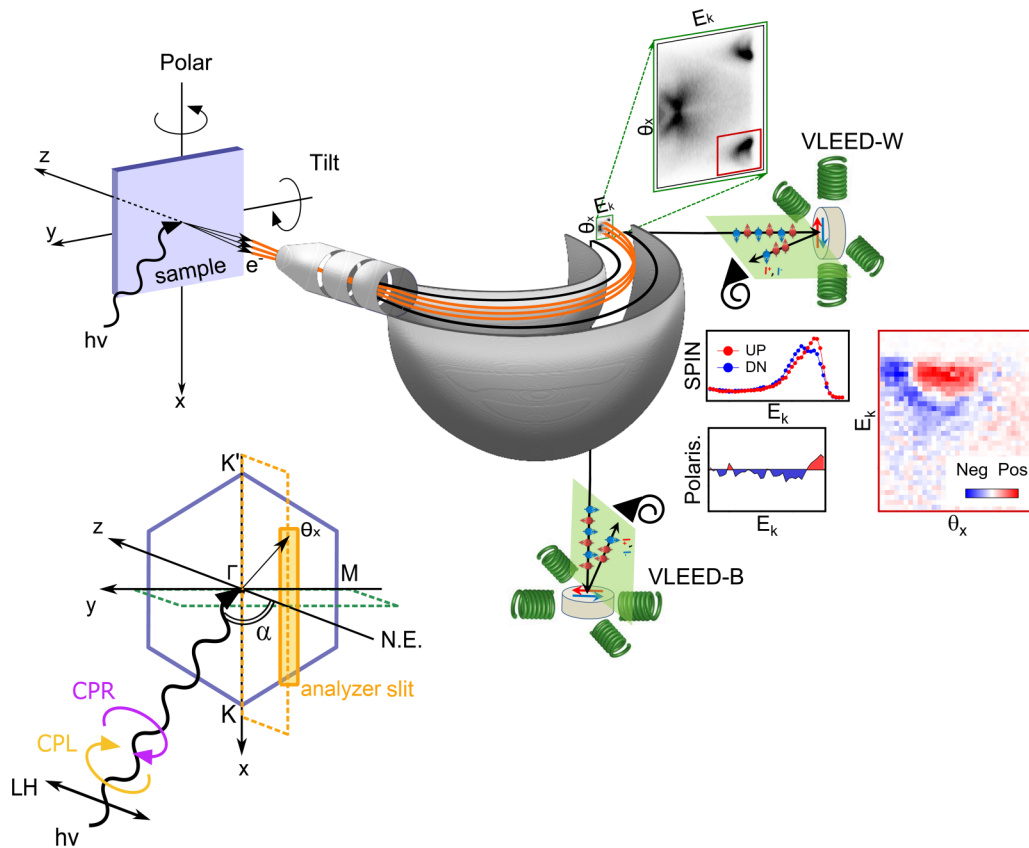


FIG. 1. Scheme of the experimental geometry at the APE-LE beamline. The accumulation ring lies in the  $yz$  plane. The photon beam is impinging the sample at an angle  $\alpha = 45^\circ$  with respect to the normal emission N.E. (i.e., the axis of the ARPES detector entrance optics). LH, CPR, and CPL light polarizations have been exploited to investigate the band structure of  $2H\text{-NbSe}_2$ . The sample is hosted on a manipulator with 5 degrees of freedom (3 translational and 2 angular). The DA30 Scienta analyzer is mounted with the slit parallel to the  $x$  axis (i.e., perpendicular to the LH polarization vector) and collects the photoelectrons emitted at angle  $\Theta_x$  within  $30^\circ$  maximum acceptance. The orange lines mark the photoelectron beam trajectory inside the analyzer body reaching the MCP where the ARPES spectrum is collected. The ARPES analyzer is fitted with a very low-energy electron diffraction (VLEED) spin polarimeter [26,28,29]. There are two VLEED scattering chambers (i.e., VLEED-B and VLEED-W) mounted at  $90^\circ$  with respect to each other providing the three components of the SP vector. Once filtered in energy and momentum, the photoelectron beam enters the VLEED scattering chambers through two independent apertures hosted on the DA30 exit plane (black trajectories). VLEED-W measures the SP component along the  $x$ -axis, which lays in the sample surface parallel to the analyzer slit. VLEED-B probes the other in-plane component along the  $y$ -axis. Both VLEED-W and VLEED-B measure the out-of-plane SP component, allowing cross-normalization of the data. Therefore, the full 3D vectorial SP can be reconstructed.

[32,50,58–60]. Colored lines on the FS in Fig. 2(b) identify the directions ( $K'$ - $\Gamma$ - $K$ ,  $K$ - $M$ - $K'$ , and  $\Gamma$ - $M$ ), where respective  $E_B$  versus  $k_{\parallel}$  in Fig. 2(c) were measured.

In principle,  $2H$ -NbSe<sub>2</sub> displays spin-polarized states only in the monolayer limit, where the centrosymmetric symmetry of the crystal is broken. The strong SOC drives the SP to be mainly oriented orthogonal to the surface layer (out-of-plane) [5,61,62] with the characteristic spin-valley locking texture [63–66]. However, the SARPES capability to probe nonzero spin polarization has been demonstrated in several bulk  $2H$ -structured TMDC systems [11,32,67,68], including  $2H$ -NbSe<sub>2</sub> [69]. In these layered systems, the bulk unit cell (centrosymmetric as a whole) can be regarded as two subunits, which locally breaks the inversion symmetry, i.e., two monolayers 180° rotated with respect to each other. The weak van der Waals interlayer coupling causes the electronic wave functions at the Brillouin zone boundaries to be strongly localized within each building-block layer, experiencing a crystal field where the inversion symmetry is locally broken. The spin de-

generacy is lifted and the system hosts momentum-dependent spin-polarized electronic states, which are spatially localized in the real space within each layer. In particular, opposite spin texture will be associated with two adjacent layer in the real space, and the spin polarization is compensated and vanishes when the bulk centrosymmetric unit cell is considered, as required by the inversion symmetry of the bulk space group. This layered-locked spin texture has been addressed as *hidden spin polarization* [70] and can be probed by SARPES thanks to the high surface sensitivity inherent to the photoemission technique. The short escape depth of photoelectrons in the VUV-XUV photon energy range (i.e.,  $\sim 5$  Å) allows us to probe only the first few layers of exfoliated  $2H$ -NbSe<sub>2</sub> bulk crystals, and the measured SP will be a finite value resulting from the superposition of such a layer-locked spin texture [32,67,69]. In particular, the trigonally warped contours encircling  $K$  and  $K'$  points in Fig. 2(b) display a strong out-of-plane spin polarization and provide a *good case study* to directly compare SP measurements and CD effects in ARPES.

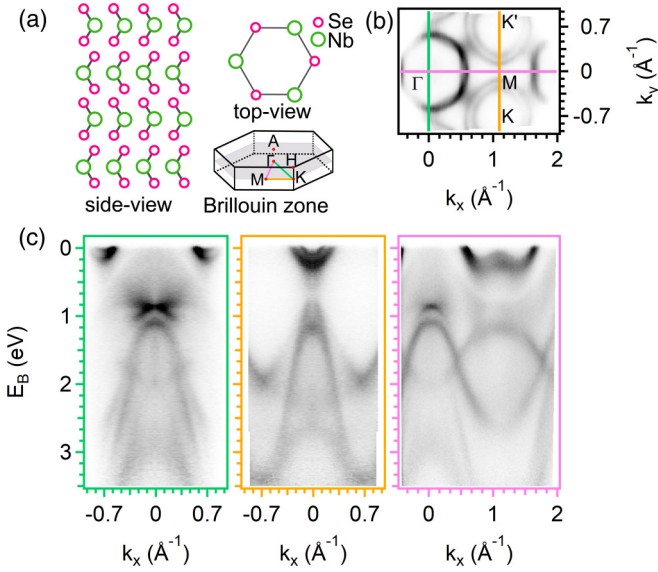


FIG. 2. (a) 2H-NbSe<sub>2</sub> crystal structure and the Brillouin zone (BZ); the gray area in the BZ marks the  $\Gamma$ -K-M plane probed by 70 eV photon energy, and the colored lines indicate the high-symmetry directions along which we extracted the  $E_B$  vs  $k_{\parallel}$  ARPES spectra reported in (c). (b) The corresponding Fermi surface acquired with  $h\nu = 70$  eV linearly horizontal (LH) polarized light. The colored lines mark where the  $E_B$  vs  $k_{\parallel}$  dispersions have been extracted. (c) Band dispersions  $E_B$  vs  $k_{\parallel}$  along the high symmetric directions of 2H-NbSe<sub>2</sub>(0001). Panels from left to right:  $K'-\Gamma-K$  (green),  $K'-M-K$  (yellow), and  $\Gamma-M$  (pink).

The CD-ARPES measured with  $h\nu = 70$  eV along  $K'-\Gamma-K$  is shown in Fig. 3. The intense pockets at the Fermi level correspond to the out-of-plane spin-polarized trigonally warped Fermi contours discussed above. The CD is quite large and displays a clear left-to-right asymmetry. The zero CD signal

at  $\Gamma$  is consistent with  $k_x = 0$  being a nodal plane in our experimental geometry [46,71,72]. The MEE transfer function giving rise to such a large CD effect [Fig. 3(d)] reflects the handedness of the experimental geometry. Panels (e) and (f) in Fig. 3 sketch the experimental geometry of the APE-LE setup. The incoming photon beam and the sample normal emission direction [i.e., the green arrow parallel to the  $z$  axis of Figs. 3(e) and 3(f)] define the incidence plane (the  $yz$  plane, marked by the green dashed rectangle). In our case, the analyzer slit (marked in orange in Fig. 3) is perpendicular to such a plane and parallel to the  $x$  axis. The SP vector is mainly oriented along the  $z$ -axis (i.e., the “out-of-plane” polarization direction), while the vectorial SP measurements show a negligible contribution along the in-plane components. The photoelectrons emitted at  $\pm k$  lying in the  $xz$  orange dashed plane of Figs. 3(e) and 3(f) are linked through a reflection operation with respect to the incidence plane. The light helicity will be reversed by such an operation. The CD is therefore an odd function displaying the opposite sign for opposite momenta. However, the CD intensity measured for our sample is not monotonic with the  $k$  momentum, as would be expected if the MEE was dominated just by geometry [22,35]. In fact, the CD displayed by NbSe<sub>2</sub> has a complex  $k$ -dependence, reversing its sign several times along the  $K-\Gamma-K'$  direction, indicating that the CD reflects the symmetry properties of the initial states, as expected, on top of the experimental chirality.

Figure 4 compares the CD-ARPES measured with  $h\nu = 25$  eV along  $K'-M-K$  with the SARPES probed with the same photon energy and LH polarization. The four dispersive bands crossing the Fermi level correspond to the trigonally warped pockets encircling the  $K$  and  $K'$  inequivalent points [Fig. 4(d)]. The CD shows a sign reversal across the  $M$  point: the null CD asymmetry at the  $M$  point is further proof of the nodal plane mentioned above [46,71,72]. The band structure shows a strong dependence on the light helicity immediately away from the nodal plane. In particular, the CD asymmetry

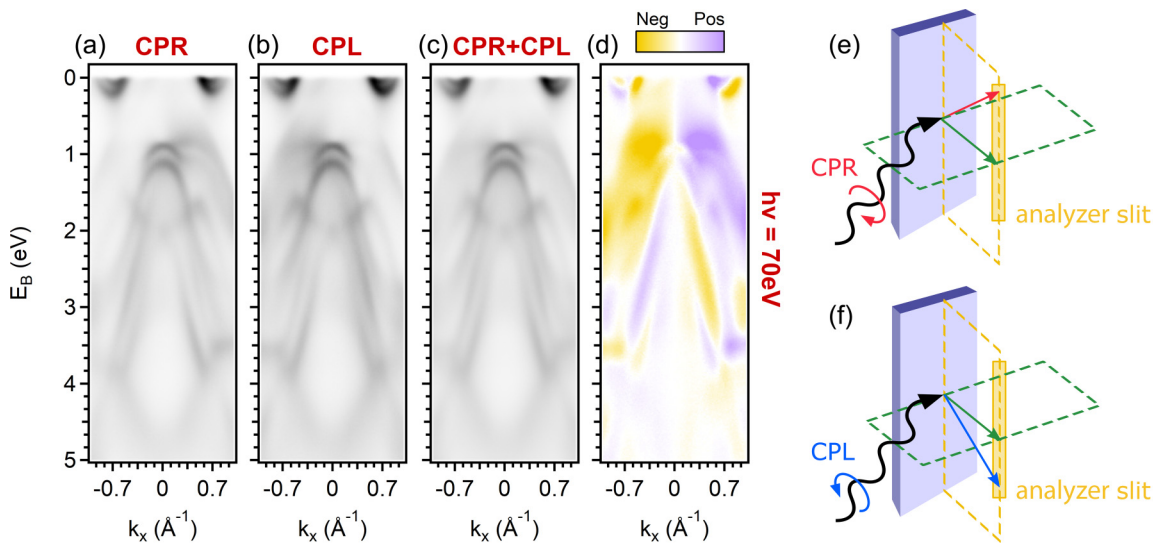


FIG. 3. ARPES and CD-ARPES spectra of the NbSe<sub>2</sub> electronic bands measured at 70 eV photon energy along the  $K-\Gamma-K'$  high-symmetry direction. (a) Circular polarization right (CPR) and (b) circular polarization left (CPL). Parts (c) and (d) reports the sum (CPR+CPL) and the circular dichroic ARPES spectrum, respectively. The experimental geometry is sketched in panels (e) and (f) for the CPR-CPL light polarization, respectively.



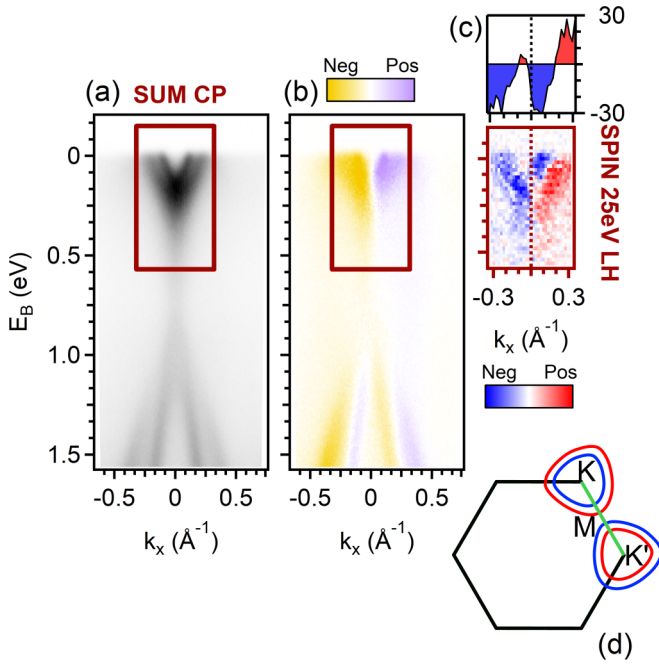


FIG. 4. ARPES, CD-ARPES, and SARPES spectra of the spin-polarized pockets along the  $K$ - $M$ - $K'$  high-symmetry direction. The ARPES data were acquired at  $h\nu = 25$  eV. (a) Sum spectra (CPR+CPL). (b) Circular dichroic ARPES spectrum. (c) SARPES data measured along the out-of-plane spin component with 25 eV linearly polarized light. (d) Sketch of the Brillouin zone and of the spin-polarized pockets under investigation. The green line marks the direction along which the measurements were performed. The brown rectangles in panels (a) and (b) indicate the corresponding area where the SARPES map in (c) was acquired.

is large close to the  $M$  point [i.e., close to  $k_x = 0$  Å<sup>-1</sup> of Fig. 4(b)] and decreases for higher absolute  $k_x$  values. The left-to-right intensity asymmetry arising from the two opposite light helicities is consistent with the so called spin-valley locking of the pockets observed by pump-probe [66] and photoluminescence experiments [64,65]. It has recently been proposed to reflect either the local chirality at the inequivalent  $K'$  and  $K$  points [73] or the point-group symmetries within the layer [74]. However, the CD signal strongly deviates from the expected initial state SP as well as from the measured spin-resolved spectra reported in Fig. 4(c). At the  $M$  time-reversal invariant moment (TRIM) point [at  $k_x = 0$  Å<sup>-1</sup> of Fig. 4(c)], the time-reversal symmetry imposes the spin degeneracy and the spin signal gives zero intensity. Away from the  $M$  point, the spin of the metallic state undergoes four sign reversals as  $k_x$  spans from negative to positive values: it starts from a negative value [blue in panel (c) of Fig. 4] for the inner Fermi surface sheet around the  $K$  point, which crosses  $E_F$  at  $k_x = -0.3$  Å<sup>-1</sup>; the SP signal changes to positive values (red) for the outer trigonal band that circles the  $K$  point and turns to zero at the  $M$  point. The SP trend is reversed for positive  $k_x$ , consistently with the threefold rotational symmetry of the lattice and the time-reversal symmetry [i.e., positive (negative) for the inner (outer) trigonal Fermi contours around  $K'$ ] [61]. Notably, the spin-resolved data are consistent with the spin valley locking texture predicted for this material and reported

in the literature [63,69]. On the contrary, the CD-ARPES is positive (negative) for positive (negative) values of  $k_x$ , respectively.

The different patterns of CD and SP are even more evident in the data set reported in Fig. 5, which shows CD and SARPES data as measured with different photon energies. The NbSe<sub>2</sub> were probed along the  $\Gamma$ - $K'$  symmetry direction with linear horizontal polarization. The CD exhibits a quite complex behavior, displaying a sizable intensity also for bands close to the  $\Gamma$  point where the spin polarization is expected to be negligible. Moreover, the CD relative to the spin-polarized Fermi contours reverses its sign between 33 and 44 eV photon energies. This behavior of CD data has been observed on several systems such as the Rashba state in BiTeX ( $X = \text{I, Br, Cl}$ ) related compounds [42,43] and topological insulators [46,72,75–77]. The origin of such a large MEE dependence upon excitation energy is not quantitatively understood: it has been attributed to initial-state [75,76,78] or final-state effects [46,72].

The SP measurement is much less affected by the MEE transfer function, and reliably identifies the spin character of the electron states. The second row of Fig. 5 shows the spin-filtered energy distribution curves (EDCs), and the third row reports the respective spin polarization  $P_z$ . For direct comparison, the bottom row compares the CD signal extracted at the same  $k_{\parallel}$  where SP was measured. For the investigated energies, the SP is consistently sizable, ranging from 20% to 30% near the Fermi level, and it never shows a sign reversal in contrast to the CD. These findings along with those reported on Bi<sub>2</sub>Se<sub>3</sub> [44] demonstrate the impossibility to infer the spin properties of the materials by means of CD-ARPES alone [35]. The fact that large CD is observed also for states characterized by weak spin-orbit coupling is not surprising: it has already been reported in systems with weak SOC such as the Cu(111) Shockley surface state and the  $\pi$  bands of graphite [18,37,41]. The large CD of Cu(111)  $p_z$  surface states was attributed to MEE involving  $d$ -character of the final states [41], which is suggestive for the interpretation of our results as the Se  $4p_z$  derived bands near the  $\Gamma$  point are typically excited to the  $d$ -like final states (rather than  $s$ -like) in the photon energy range used in this study [44].

Overall, these results strongly indicate that the spin properties of complex materials cannot be derived from CD-ARPES data, and that the correct interpretation of the dichroism requires us to carefully model the MEE transfer function of the given experiment [79]. The radial part or “shape” of the initial state wave function enters the MEE and the resulting transfer function which influences the CD. The SP of the initial state does not determine the shape of the wave function, unless perhaps when exchange interaction is very large as in ferromagnets, and it can be detected by SP measurements, being only weakly affected by the ubiquitous MEE.

### III. CONCLUSIONS

In conclusion, we investigated the valence-band states of the NbSe<sub>2</sub> by SARPES measurements as a function of the photon energy and polarization disentangling the large dichroic signals, which are a manifestation of MEE, from the spin polarization. MEE determines the effective transfer

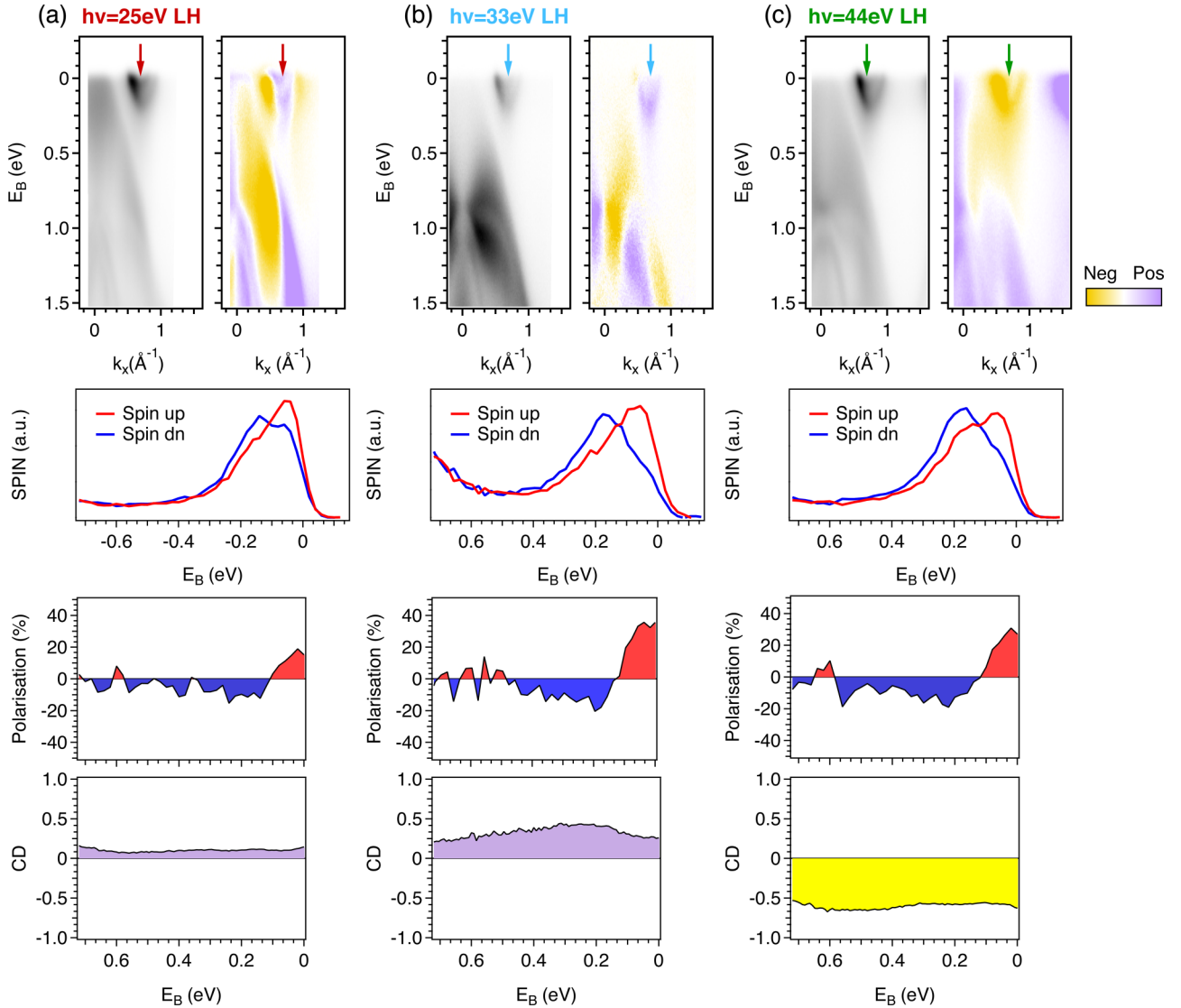


FIG. 5. ARPES, circular dichroic ARPES (CD-ARPES), and SARPES measured along the  $\Gamma$ - $K'$  direction at different photon energies: (a) 25 eV, (b) 33 eV, and (c) 44 eV. The ARPES and SARPES data were measured with linearly horizontal polarized light. The colored arrows on the ARPES and CD-ARPES spectra mark the  $k_x$  momenta where the spin texture has been probed. Top row reports the ARPES and CD-ARPES spectra, middle panels show the spin-filtered EDCs and the corresponding out-of-plane SP values. Bottom row reports the CD signal obtained from the CD-ARPES at the same  $k_{||}$  value where the SARPES was performed.

function from  $A(\mathbf{k}, \omega)$  to  $I_{ph}(\mathbf{k}, \omega)$  that is also affected by the chirality of the experimental setup. The measured CD strongly depends on the photon energy value and manifests itself as sign reversal of the  $I_{ph}(\mathbf{k}, \omega)$ . Conversely, the SP data emerge as a direct signature of the spin texture at all explored energies and LH light polarization. The variations of SP values obtained (20–30 %) can be interpreted as a manifestation of the hidden spin polarization in the 2H-NbSe<sub>2</sub> system [69] combined with the changes of escape depth  $\lambda$  for photoelectrons excited by different photon energies (i.e.,  $\lambda \sim 8$ –5 Å for kinetic energies changing from  $\sim 20$  eV to  $\sim 40$  eV) [80]. As a result, the electrons photoemitted by different subunits of the unit cell interfere, and sizable variations in the degree of spin polarization are obtained, in agreement with other studies [32,67–70]. By referring to the atomic model, one could infer that CD reflects alignment of the initial states, but only SARPES can reflect unambiguously their orientation,

i.e., their SP. The intensities of each spin component of the photoemission peaks may actually be affected by MEE, too. Our SP data show that such changes are small enough in the chosen geometry to authorize the interpretation of SP in terms of initial-state properties. The fact that almost an entirely out-of-plane component of SP is measured in NbSe<sub>2</sub> furthermore proves that the measurement is a good characterization of the initial state. The large MEE on  $I_{ph}(\mathbf{k}, \omega)$ , and the escape depth considerations, must nevertheless be considered when quantitatively comparing experimental SP values with theoretical expectations, as well as with data obtained in different setups as the possible mismatches do not necessarily imply material or sample specific features [11].

We have shown, on the other hand, that reliable information on the spin texture of 2H-NbSe<sub>2</sub> cannot be derived from CD-ARPES. The exploitation of SARPES experiments in carefully controlled geometries is needed to assess the

spin polarization of electron states and this result is general. Although photoemission intensities can influence the absolute value of the measured SP, the lack of explicit SP measurements cannot be replaced by circular or linear dichroism when measuring band states. Significant efforts are currently being invested in simulating the effective intensities of SARPEs of quantum materials in a given experimental setup for a given sample orientation and overall measurement conditions.

Shortcuts in the interpretation of SP of the extended states from CD-ARPES intensities are definitely not justified.

### ACKNOWLEDGMENT

This work has been performed in the framework of the Nanoscience Foundry and Fine Analysis (NFFA-MUR Italy Progetti Internazionali) facility.

- [1] K. Sakamoto, T.-H. Kim, T. Kuzumaki, B. Müller, Y. Yamamoto, M. Ohtaka, J. R. Osiecki, K. Miyamoto, Y. Takeichi, A. Harasawa *et al.*, Valley spin polarization by using the extraordinary Rashba effect on silicon, *Nat. Commun.* **4**, 2073 (2013).
- [2] K. Sakamoto, T. Oda, A. Kimura, K. Miyamoto, M. Tsujikawa, A. Imai, N. Ueno, H. Namatame, M. Taniguchi, P. Eriksson *et al.*, Abrupt Rotation of the Rashba Spin to the Direction Perpendicular to the Surface, *Phys. Rev. Lett.* **102**, 096805 (2009).
- [3] Z.-H. Zhu, G. Levy, B. Ludbrook, C. Veenstra, J. Rosen, R. Comin, D. Wong, P. Dosanjh, A. Ubaldini, P. Syers *et al.*, Rashba Spin-Splitting Control at the Surface of the Topological Insulator Bi<sub>2</sub>Se<sub>3</sub>, *Phys. Rev. Lett.* **107**, 186405 (2011).
- [4] I. Vobornik, G. Panaccione, J. Fujii, Z.-H. Zhu, F. Offi, B. R. Salles, F. Borgatti, P. Torelli, J. P. Rueff, D. Ceolin *et al.*, Observation of distinct bulk and surface chemical environments in a topological insulator under magnetic doping, *J. Phys. Chem. C* **118**, 12333 (2014).
- [5] H. Zhang, C.-X. Liu, X.-L. Qi, X. Dai, Z. Fang, and S.-C. Zhang, Topological insulators in Bi<sub>2</sub>Se<sub>3</sub>, Bi<sub>2</sub>Te<sub>3</sub> and Sb<sub>2</sub>Te<sub>3</sub> with a single Dirac cone on the surface, *Nat. Phys.* **5**, 438 (2009).
- [6] S. Hüfner, *Very High Resolution Photoelectron Spectroscopy* (Springer-Verlag, Berlin, Heidelberg, 2007), Vol. 715.
- [7] A. Damascelli, Probing the electronic structure of complex systems by ARPES, *Phys. Scr.* **2004**, 61 (2004).
- [8] A. Damascelli, Z. Hussain, and Z.-X. Shen, Angle-resolved photoemission studies of the cuprate superconductors, *Rev. Mod. Phys.* **75**, 473 (2003).
- [9] J. Sánchez-Barriga, J. Fink, V. Boni, I. Di Marco, J. Braun, J. Minár, A. Varykhalov, O. Rader, V. Bellini, F. Manghi *et al.*, Strength of Correlation Effects in the Electronic Structure of Iron, *Phys. Rev. Lett.* **103**, 267203 (2009).
- [10] F. Da Pieve and P. Krüger, Real-space Green's function approach to angle-resolved resonant photoemission: Spin polarization and circular dichroism in itinerant magnets, *Phys. Rev. B* **88**, 115121 (2013).
- [11] E. Razzoli, T. Jaouen, M.-L. Mottas, B. Hildebrand, G. Monney, A. Pisoni, S. Muff, M. Fanciulli, N. C. Plumb, V. Rogalev *et al.*, Selective Probing of Hidden Spin-Polarized States in Inversion-Symmetric Bulk MoS<sub>2</sub>, *Phys. Rev. Lett.* **118**, 086402 (2017).
- [12] K. Yaji, K. Kuroda, S. Toyohisa, A. Harasawa, Y. Ishida, S. Watanabe, C. Chen, K. Kobayashi, F. Komori, and S. Shin, Spin-dependent quantum interference in photoemission process from spin-orbit coupled states, *Nat. Commun.* **8**, 14588 (2017).
- [13] H. Bentmann, H. Maaß, E. E. Krasovskii, T. R. F. Peixoto, C. Seibel, M. Leandersson, T. Balasubramanian, and F. Reinert, Strong Linear Dichroism in Spin-Polarized Photoemission from Spin-Orbit-Coupled Surface States, *Phys. Rev. Lett.* **119**, 106401 (2017).
- [14] K. Miyamoto, H. Wortelen, T. Okuda, J. Henk, and M. Donath, Circular-polarized-light-induced spin polarization characterized for the Dirac-cone surface state at W (110) with C<sub>2v</sub> symmetry, *Sci. Rep.* **8**, 10440 (2018).
- [15] N. Cherepkov, Spin polarisation of photoelectrons ejected from unpolarised atoms, *J. Phys. B* **12**, 1279 (1979).
- [16] N. A. Cherepkov, Origin of magnetic dichroism in angular-resolved photoemission from ferromagnets, *Phys. Rev. B* **50**, 13813 (1994).
- [17] G. Schönhense, Angular Dependence of the Polarization of Photoelectrons Ejected by Plane-Polarized Radiation from Argon and Xenon Atoms, *Phys. Rev. Lett.* **44**, 640 (1980).
- [18] G. Schönhense, C. Westphal, J. Bansmann, and M. Getzlaff, Circular dichroism in photoemission from nonmagnetic, low-Z solids: A conspicuous effect of the photon spin, *Europhys. Lett.* **17**, 727 (1992).
- [19] K. Blum, *Density Matrix Theory and Applications* (Springer-Verlag, Berlin, Heidelberg, 2012), Vol. 64.
- [20] N. Cherepkov and V. Kuznetsov, Optical activity of polarised atoms, *J. Phys. B* **22**, L405 (1989).
- [21] L. Baumgarten, C. M. Schneider, H. Petersen, F. Schäfers, and J. Kirschner, Magnetic X-Ray Dichroism in Core-Level Photoemission from Ferromagnets, *Phys. Rev. Lett.* **65**, 492 (1990).
- [22] D. Venus, Magnetic circular dichroism in angular distributions of core-level photoelectrons, *Phys. Rev. B* **48**, 6144 (1993).
- [23] G. Rossi, F. Sirotti, N. Cherepkov, F. C. Farnoux, and G. Panaccione, 3p fine structure of ferromagnetic Fe and Co from photoemission with linearly polarized light, *Solid State Commun.* **90**, 557 (1994).
- [24] G. Rossi, G. Panaccione, F. Sirotti, and N. A. Cherepkov, Magnetic-field-averaged photoemission experiments with variable chirality, *Phys. Rev. B* **55**, 11483 (1997).
- [25] M. Hoesch, T. Greber, V. Petrov, M. Muntwiler, M. Hengsberger, W. Auwärter, and J. Osterwalder, Spin-polarized Fermi surface mapping, *J. Electron Spectrosc. Relat. Phenom.* **124**, 263 (2002).
- [26] T. Okuda, K. Miyamoto, A. Kimura, H. Namatame, and M. Taniguchi, A double VLEED spin detector for high-resolution three dimensional spin vectorial analysis of anisotropic Rashba spin splitting, *J. Electron Spectrosc. Relat. Phenom.* **201**, 23 (2015).
- [27] C. Tusche, A. Krasnyuk, and J. Kirschner, Spin resolved bandstructure imaging with a high resolution momentum microscope, *Ultramicroscopy* **159**, 520 (2015).

- [28] K. Yaji, A. Harasawa, K. Kuroda, S. Toyohisa, M. Nakayama, Y. Ishida, A. Fukushima, S. Watanabe, C. Chen, F. Komori *et al.*, High-resolution three-dimensional spin-and angle-resolved photoelectron spectrometer using vacuum ultraviolet laser light, *Rev. Sci. Instrum.* **87**, 053111 (2016).
- [29] C. Bigi, P. K. Das, D. Benedetti, F. Salvador, D. Krizmancic, R. Sergo, A. Martin, G. Panaccione, G. Rossi, J. Fujii *et al.*, Very efficient spin polarization analysis (VESPA): New exchange scattering-based setup for spin-resolved ARPES at APE-NFFA beamline at Elettra, *J. Synchrotron Radiat.* **24**, 750 (2017).
- [30] D. Hsieh, Y. Xia, D. Qian, L. Wray, J. Dil, F. Meier, J. Osterwalder, L. Patthey, J. Checkelsky, N. P. Ong *et al.*, A tunable topological insulator in the spin helical Dirac transport regime, *Nature (London)* **460**, 1101 (2009).
- [31] S.-K. Mo, C. Hwang, Y. Zhang, M. Fanciulli, S. Muff, J. H. Dil, Z.-X. Shen, and Z. Hussain, Spin-resolved photoemission study of epitaxially grown MoSe<sub>2</sub> and WSe<sub>2</sub> thin films, *J. Phys.: Condens. Matter* **28**, 454001 (2016).
- [32] J. M. Riley, F. Mazzola, M. Dendzik, M. Michiardi, T. Takayama, L. Bawden, C. Granerød, M. Leandersson, T. Balasubramanian, M. Hoesch *et al.*, Direct observation of spin-polarized bulk bands in an inversion-symmetric semiconductor, *Nat. Phys.* **10**, 835 (2014).
- [33] R. Vidal, H. Bentmann, T. Peixoto, A. Zeugner, S. Moser, C.-H. Min, S. Schatz, K. Kißner, M. Ünzelmann, C. Fornari *et al.*, Surface states and Rashba-type spin polarization in antiferromagnetic MnBi<sub>2</sub>Te<sub>4</sub> (0001), *Phys. Rev. B* **100**, 121104(R) (2019).
- [34] J. Kessler, *Polarized Electrons* (Springer-Verlag, Berlin, Heidelberg, 1985), Vol. 1.
- [35] Y. H. Wang, D. Hsieh, D. Pilon, L. Fu, D. R. Gardner, Y. S. Lee, and N. Gedik, Observation of a Warped Helical Spin Texture in Bi<sub>2</sub>Se<sub>3</sub> from Circular Dichroism Angle-Resolved Photoemission Spectroscopy, *Phys. Rev. Lett.* **107**, 207602 (2011).
- [36] M. Bahramy, P. King, A. De La Torre, J. Chang, M. Shi, L. Patthey, G. Balakrishnan, P. Hofmann, R. Arita, N. Nagaosa *et al.*, Emergent quantum confinement at topological insulator surfaces, *Nat. Commun.* **3**, 1159 (2012).
- [37] B. Kim, C. H. Kim, P. Kim, W. Jung, Y. Kim, Y. Koh, M. Arita, K. Shimada, H. Namatame, M. Taniguchi *et al.*, Spin and orbital angular momentum structure of Cu (111) and Au (111) surface states, *Phys. Rev. B* **85**, 195402 (2012).
- [38] S. R. Park, J. Han, C. Kim, Y. Y. Koh, C. Kim, H. Lee, H. J. Choi, J. H. Han, K. D. Lee, N. J. Hur *et al.*, Chiral Orbital-Angular Momentum in the Surface States of Bi<sub>2</sub>Se<sub>3</sub>, *Phys. Rev. Lett.* **108**, 046805 (2012).
- [39] I. Abbati, L. Braicovich, G. Rossi, I. Lindau, U. del Pennino, and S. Nannarone, Solid-State Effects on the Valence-Band 4D-Photoionization Cross Sections at the Cooper Minimum, *Phys. Rev. Lett.* **50**, 1799 (1983).
- [40] G. Rossi, I. Lindau, L. Braicovich, and I. Abbati, Cooper-minimum effects in the photoionization cross sections of 4d and 5d electrons in solid compounds, *Phys. Rev. B* **28**, 3031 (1983).
- [41] M. Mulazzi, G. Rossi, J. Braun, J. Minár, H. Ebert, G. Panaccione, I. Vobornik, and J. Fujii, Understanding intensities of angle-resolved photoemission with circularly polarized radiation from a Cu (111) surface state, *Phys. Rev. B* **79**, 165421 (2009).
- [42] A. Crepaldi, F. Cilento, M. Zaccagna, M. Zonno, J. Johannsen, C. Tournier-Colletta, L. Moreschini, I. Vobornik, F. Bondino, E. Magnano *et al.*, Momentum and photon energy dependence of the circular dichroic photoemission in the bulk Rashba semiconductors BiTeX (X= I, Br, Cl), *Phys. Rev. B* **89**, 125408 (2014).
- [43] L. Bawden, J. M. Riley, C. H. Kim, R. Sankar, E. J. Monkman, D. E. Shai, H. I. Wei, E. B. Lochocki, J. W. Wells, W. Meevasana *et al.*, Hierarchical spin-orbital polarization of a giant Rashba system, *Sci. Adv.* **1**, e1500495 (2015).
- [44] J. Sánchez-Barriga, A. Varykhalov, J. Braun, S.-Y. Xu, N. Alidoust, O. Kornilov, J. Minár, K. Hummer, G. Springholz, G. Bauer *et al.*, Photoemission of Bi<sub>2</sub>Se<sub>3</sub> with Circularly Polarized Light: Probe of Spin Polarization or Means for Spin Manipulation? *Phys. Rev. X* **4**, 011046 (2014).
- [45] M. Mulazzi, M. Hochstrasser, M. Corso, I. Vobornik, J. Fujii, J. Osterwalder, J. Henk, and G. Rossi, Matrix element effects in angle-resolved valence band photoemission with polarized light from the Ni (111) surface, *Phys. Rev. B* **74**, 035118 (2006).
- [46] M. Scholz, J. Sánchez-Barriga, J. Braun, D. Marchenko, A. Varykhalov, M. Lindroos, Y. J. Wang, H. Lin, A. Bansil, J. Minár *et al.*, Reversal of the Circular Dichroism in Angle-Resolved Photoemission from Bi<sub>2</sub>Te<sub>3</sub>, *Phys. Rev. Lett.* **110**, 216801 (2013).
- [47] H. Hedayat, D. Bugini, H. Yi, C. Chen, X. Zhou, G. Cerullo, C. Dallera, and E. Carbone, Ultrafast evolution of bulk, surface and surface resonance states in photoexcited Bi<sub>2</sub>Te<sub>3</sub>, *Sci. Rep.* **11**, 4924 (2021).
- [48] M. M. Ugeda, A. J. Bradley, Y. Zhang, S. Onishi, Y. Chen, W. Ruan, C. Ojeda-Aristizabal, H. Ryu, M. T. Edmonds, H.-Z. Tsai *et al.*, Characterization of collective ground states in single-layer NbSe<sub>2</sub>, *Nat. Phys.* **12**, 92 (2016).
- [49] S. Borisenko, A. Kordyuk, V. Zabolotnyy, D. Inosov, D. Evtushinsky, B. Büchner, A. Yaresko, A. Varykhalov, R. Follath, W. Eberhardt *et al.*, Two Energy Gaps and Fermi-Surface “Arcs” in NbSe<sub>2</sub>, *Phys. Rev. Lett.* **102**, 166402 (2009).
- [50] R. Corcoran, P. Meeson, Y. Onuki, P.-A. Probst, M. Springford, K. Takita, H. Harima, G. Guo, and B. Gyorffy, Quantum oscillations in the mixed state of the type ii superconductor 2H-NbSe<sub>2</sub>, *J. Phys.: Condens. Matter* **6**, 4479 (1994).
- [51] T. Yokoya, T. Kiss, A. Chainani, S. Shin, M. Nohara, and H. Takagi, Fermi surface sheet-dependent superconductivity in 2H-NbSe<sub>2</sub>, *Science* **294**, 2518 (2001).
- [52] M. Johnson and R. H. Silsbee, Interfacial Charge-Spin Coupling: Injection and Detection of Spin Magnetization in Metals, *Phys. Rev. Lett.* **55**, 1790 (1985).
- [53] S. A. Wolf, A. Y. Chtchelkanova, and D. M. Treger, Spintronics: A retrospective and perspective, *IBM J. Res. Dev.* **50**, 101 (2006).
- [54] A. Manchon, H. C. Koo, J. Nitta, S. Frolov, and R. Duine, New perspectives for Rashba spin-orbit coupling, *Nat. Mater.* **14**, 871 (2015).
- [55] hq graphene, <http://www.hqgraphene.com/>.
- [56] G. Panaccione, I. Vobornik, J. Fujii, D. Krizmancic, E. Annese, L. Giovannelli, F. Maccheronzi, F. Salvador, A. De Luisa, D. Benedetti *et al.*, Advanced photoelectric effect experiment beamline at Elettra: A surface science laboratory coupled with synchrotron radiation, *Rev. Sci. Instrum.* **80**, 043105 (2009).
- [57] K. Rossnagel, O. Seifarth, L. Kipp, M. Skibowski, D. Voß, P. Krüger, A. Mazur, and J. Pollmann, Fermi surface of 2H-NbSe<sub>2</sub>



- and its implications on the charge-density-wave mechanism, *Phys. Rev. B* **64**, 235119 (2001).
- [58] N. Doran, D. Titterton, B. Ricco, and G. Wexler, A tight binding fit to the bandstructure of NbSe<sub>2</sub> and NbS<sub>2</sub>, *J. Phys. C* **11**, 685 (1978).
- [59] H. Zeng, G.-B. Liu, J. Dai, Y. Yan, B. Zhu, R. He, L. Xie, S. Xu, X. Chen, W. Yao *et al.*, Optical signature of symmetry variations and spin-valley coupling in atomically thin tungsten dichalcogenides, *Sci. Rep.* **3**, 1608 (2013).
- [60] Y. Noat, J. Silva-Guillén, T. Cren, V. Cherkez, C. Brun, S. Pons, F. Debontridder, D. Roditchev, W. Sacks, L. Cario *et al.*, Quasiparticle spectra of NbSe<sub>2</sub>: Two-band superconductivity and the role of tunneling selectivity, *Phys. Rev. B* **92**, 134510 (2015).
- [61] M. Nagano, A. Kodama, T. Shishidou, and T. Oguchi, A first-principles study on the Rashba effect in surface systems, *J. Phys.: Condens. Matter* **21**, 064239 (2009).
- [62] W.-Y. He, B. T. Zhou, J. J. He, N. F. Yuan, T. Zhang, and K. T. Law, Magnetic field driven nodal topological superconductivity in monolayer transition metal dichalcogenides, *Commun. Phys.* **1**, 40 (2018).
- [63] P. Dey, L. Yang, C. Robert, G. Wang, B. Urbaszek, X. Marie, and S. A. Crooker, Gate-Controlled Spin-Valley Locking of Resident Carriers in WSe<sub>2</sub> Monolayers, *Phys. Rev. Lett.* **119**, 137401 (2017).
- [64] H. Zeng, J. Dai, W. Yao, D. Xiao, and X. Cui, Valley polarization in MoS<sub>2</sub> monolayers by optical pumping, *Nat. Nanotechnol.* **7**, 490 (2012).
- [65] T. Cao, G. Wang, W. Han, H. Ye, C. Zhu, J. Shi, Q. Niu, P. Tan, E. Wang, B. Liu *et al.*, Valley-selective circular dichroism of monolayer molybdenum disulphide, *Nat. Commun.* **3**, 887 (2012).
- [66] R. Bertoni, C. W. Nicholson, L. Waldecker, H. Hübener, C. Monney, U. De Giovannini, M. Puppini, M. Hoesch, E. Springate, R. T. Chapman *et al.*, Generation and Evolution of Spin-, Valley-, and Layer-Polarized Excited Carriers in Inversion-Symmetric WSe<sub>2</sub>, *Phys. Rev. Lett.* **117**, 277201 (2016).
- [67] M. Gehlmann, I. Aguilera, G. Bihlmayer, E. Młyńczak, M. Eschbach, S. Döring, P. Gospodarič, S. Cramm, B. Kardynał, L. Plucinski *et al.*, Quasi 2d electronic states with high spin-polarization in centrosymmetric MoS<sub>2</sub> bulk crystals, *Sci. Rep.* **6**, 26197 (2016).
- [68] J. Tu, X. Chen, X. Ruan, Y. Zhao, H. Xu, Z. Chen, X. Zhang, X. Zhang, J. Wu, L. He *et al.*, Direct observation of hidden spin polarization in 2h-MoTe<sub>2</sub>, *Phys. Rev. B* **101**, 035102 (2020).
- [69] L. Bawden, S. Cooil, F. Mazzola, J. Riley, L. Collins-McIntyre, V. Sunko, K. Hunvik, M. Leandersson, C. Polley, T. Balasubramanian *et al.*, Spin-valley locking in the normal state of a transition-metal dichalcogenide superconductor, *Nat. Commun.* **7**, 11711 (2016).
- [70] X. Zhang, Q. Liu, J.-W. Luo, A. J. Freeman, and A. Zunger, Hidden spin polarization in inversion-symmetric bulk crystals, *Nat. Phys.* **10**, 387 (2014).
- [71] Y. Ishida, H. Kanto, A. Kikkawa, Y. Taguchi, Y. Ito, Y. Ota, K. Okazaki, W. Malaeb, M. Mulazzi, M. Okawa *et al.*, Common Origin of the Circular-Dichroism Pattern in Angle-Resolved Photoemission Spectroscopy of SrTiO<sub>3</sub> and Cu<sub>3</sub>Bi<sub>2</sub>Se<sub>3</sub>, *Phys. Rev. Lett.* **107**, 077601 (2011).
- [72] C.-Z. Xu, Y. Liu, R. Yukawa, L.-X. Zhang, I. Matsuda, T. Miller, and T.-C. Chiang, Photoemission Circular Dichroism and Spin Polarization of the Topological Surface States in Ultrathin Bi<sub>2</sub>Te<sub>3</sub> films, *Phys. Rev. Lett.* **115**, 016801 (2015).
- [73] M. Schüller, U. De Giovannini, H. Hübener, A. Rubio, M. A. Sentef, and P. Werner, Local Berry curvature signatures in dichroic angle-resolved photoelectron spectroscopy from two-dimensional materials, *Sci. Adv.* **6**, eaay2730 (2020).
- [74] A. Ketterl, S. Otto, M. Bastian, B. Andres, C. Gahl, J. Minár, H. Ebert, J. Braun, O. E. Tereshchenko, K. A. Kokh *et al.*, Origin of spin-polarized photocurrents in the topological surface states of Bi<sub>2</sub>Se<sub>3</sub>, *Phys. Rev. B* **98**, 155406 (2018).
- [75] Z.-H. Zhu, C. N. Veenstra, G. Levy, A. Ubaldini, P. Syers, N. P. Butch, J. Paglione, M. W. Haverkort, I. S. Elfimov, and A. Damascelli, Layer-by-Layer Entangled Spin-Orbital Texture of the Topological Surface State in Bi<sub>2</sub>Se<sub>3</sub>, *Phys. Rev. Lett.* **110**, 216401 (2013).
- [76] M. Neupane, S. Basak, N. Alidoust, S.-Y. Xu, C. Liu, I. Belopolski, G. Bian, J. Xiong, H. Ji, S. Jia *et al.*, Oscillatory surface dichroism of the insulating topological insulator Bi<sub>2</sub>Te<sub>2</sub>Se, *Phys. Rev. B* **88**, 165129 (2013).
- [77] F. Vidal, M. Eddrief, B. R. Salles, I. Vobornik, E. Velez-Fort, G. Panaccione, and M. Marangolo, Photon energy dependence of circular dichroism in angle-resolved photoemission spectroscopy of Bi<sub>2</sub>Se<sub>3</sub> Dirac states, *Phys. Rev. B* **88**, 241410(R) (2013).
- [78] H. Ryu, I. Song, B. Kim, S. Cho, S. Soltani, T. Kim, M. Hoesch, C. H. Kim, and C. Kim, Photon energy dependent circular dichroism in angle-resolved photoemission from Au(111) surface states, *Phys. Rev. B* **95**, 115144 (2017).
- [79] R. P. Day, B. Zwartsenberg, I. S. Elfimov, and A. Damascelli, Computational framework chinook for angle-resolved photoemission spectroscopy, *npj Quantum Mater.* **4**, 54 (2019).
- [80] M. P. Seah and W. Dench, Quantitative electron spectroscopy of surfaces: A standard data base for electron inelastic mean free paths in solids, *Surf. Interface Anal.* **1**, 2 (1979).